2018 NA62 Status Report to the CERN SPSC

Abstract

The status of the NA62 experiment is reported. The ongoing activities on detectors and hardware are summarised and the status of the data processing is reviewed. The result from the $K^+ \to \pi^+ \nu\bar{\nu}$ analysis of the full 2016 data set is presented. Ongoing analysis on rare and forbidden decays and exotic searches are also discussed.

CERN-SPSC-2018-010 / SPSC-SR-229
11/04/2018

1 Introduction

This NA62 2018 report to the SPSC emphasizes the first result on the $K^+ \to \pi^+\nu\bar{\nu}$ analysis performed on the 2016 data set. With a sensitivity already close to the Standard Model (SM) prediction for $K^+ \to \pi^+\nu\bar{\nu}$ and a background smaller than the expected signal, the overall fundamental message from the 2016 analysis is that the NA62 decay-in-flight technique works.

The 2017 run has been successful for NA62 with a statistics collected of about 20 times the 2016 one. The data taking mainly profited of the very stable beam delivered by the SPS and of good hardware performances, after having fixed the issues affecting the 2016 data-taking. This allowed NA62 to operate in 2017 constantly at an average intensity of 60-65% of the nominal one. The NA62 is ready for the 2018 data-taking where running conditions similar to last year are expected. Eventually the statistics collected from the 2017 and 2018 run will allow NA62 to measure the $K^+ \to \pi^+\nu\bar{\nu}$ decay rate.

Important progresses have taken place at software level, with the development of a new control system based on the Atlas Tier0 production system boosting significantly the data reprocessing, and with the implementation of new offline procedures to detect and correct for hardware failures, improving the overall data quality.

Thanks to these improvements, several physics analyses are presently ongoing, spanning precision measurements of lepton universality in $K^+ \to l^+\nu$ decays, studies of lepton number and flavour violating processes and searches for exotics long living particles.

In 2017 the detector paper of NA62 has been published in JINST and the first physics paper in PLB about the search for heavy neutral leptons performed on data collected in 2015.

The document is structured as follows: Sections 2 and 3 summarise the ongoing activities on the hardware and the software, respectively; the $K^+ \to \pi^+\nu\bar{\nu}$ analysis on the 2016 data is described in section 4; Sections 5 and 6 report the status of the analysis on rare/forbidden decays and exotic searches, respectively. Finally the status of the NA62 and older data publications is presented in Section 7.

2 Detectors: Ongoing Activities

Improvements on the radiation shielding have been made during the winter shutdown. The electronics racks for the KTAG, CHANTI and GTK cooling stations were equipped with additional concrete blocks to decrease the number of single event upsets (SEUs).

At the end of 2017, two LKr calorimeter HV feedthroughs were found leaking, which resulted in a degradation of the insulating vacuum. They were successfully replaced at the beginning of 2018. The level of the LKr has been stable since the summer of 2017 and there is no need to top up the liquid krypton at this point (Figure 1). Nevertheless 400 liters of liquid krypton was bought in 2017 in order to top up the liquid krypton storage. A dedicated device has been constructed to measure the lifetime (purity) of the liquid krypton. The present plan is to validate the purity of the krypton during the spring and transfer the krypton to the storage dewar in LS2.

The 2018 run started on April 9th. The data taking will be kept stable at 60% of nominal intensity since the beginning, i.e. 2018 will start as 2017 ended. The 2018 run is 217 days, 56 days more than the 2017 run. The longer data taking period in 2018 will be managed by 17 run coordinators, supervising 54 detector experts and 137 shifters for a total of 651 shifts with two shifters each.

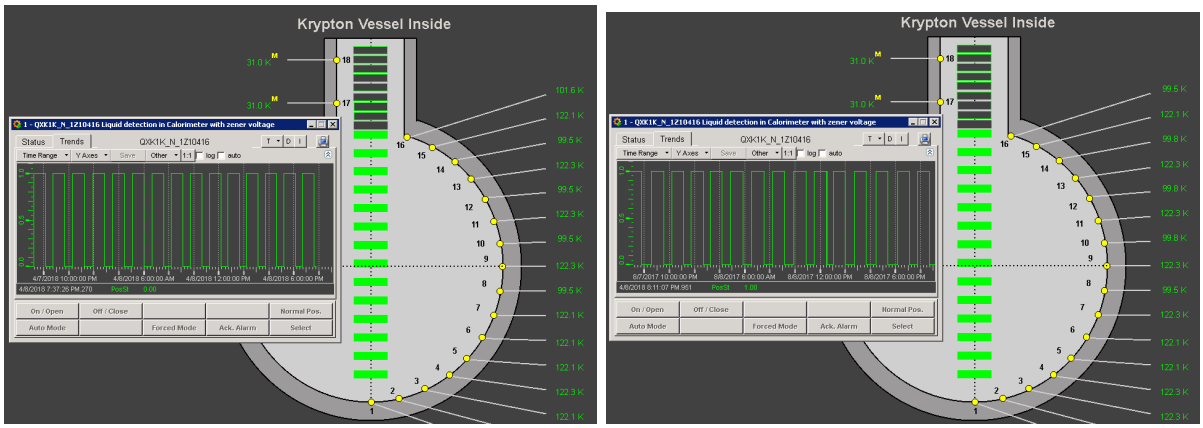

Figure 1: Liquid Krypton level indicated by Zener diode #16 (first solid green box from the top) on April 4 2018 (left) and August 7 2017 (right).

3 Data: Preparation, Processing, Quality

In the autumn of 2016, a new working group aimed to assess the quality of the collected data, to detect possible improvements for the data taking and to coordinate the offline data processing was formed, and since then we improved significantly on how we treat our data.

While working on the processing of 2016 data, several hardware issues were detected and actions were taken to reduce their impact in the future. As part of the data quality assessment, consistency checks were implemented to promptly detect corruption in the CREAM and in the GigaTracker data. These improvements were also exploited by the online data quality monitor during the 2017 run, assuring that the acquired data were of high quality, with all detectors working, and also allowing timely intervention in case of hardware failures. This is demonstrated in Fig. 2, where we show as a function of time the integrated number of kaon decays collected with all detectors working, comparing it with the delivered kaon flux. In 2017, a total of about 3×10^{12} Kaon decays in the fiducial volume were collected.

A new control system for the offline data processing, based on the Atlas Tier0 production system[1], was developed and commissioned. The processing workflow consists of 4 steps: calibration, reconstruction, filtering and post-processing. The calibration step provides channel-by-channel time offsets and other offline corrections to be applied at the reconstruction stage. Subsequently, raw data are reconstructed and events with particular signatures are selected and written to 10 output streams ("filter") for different physics analysis topics, to avoid that all the processed data have to be read by all analyses. Finally, during the post-processing, the quality of the reconstructed data sample is assessed.

A typical burst has ∼280,000 events, with a raw data size of about 3.5 GBytes. In 2017, we recorded about 300,000 good bursts and, just considering the longer data taking period, we expect around 500,000 bursts in 2018. In total for 2016, 2017, and 2018 data we expect about 3.5 PBytes of raw data and the same amount for filtered output (output of the reconstruction stage is only stored temporarily since it would add up to about 7 PBytes extra).

With the help of the CERN-IT department we understood how to improve the usage of our resources. One of the key points was the migration of the offline data processing from `lsf` to `HTCondor`, on which we had a significantly higher number of dedicated CPU cores. Furthermore,

[1]We thank the EP-ADP-CO section members for their support.

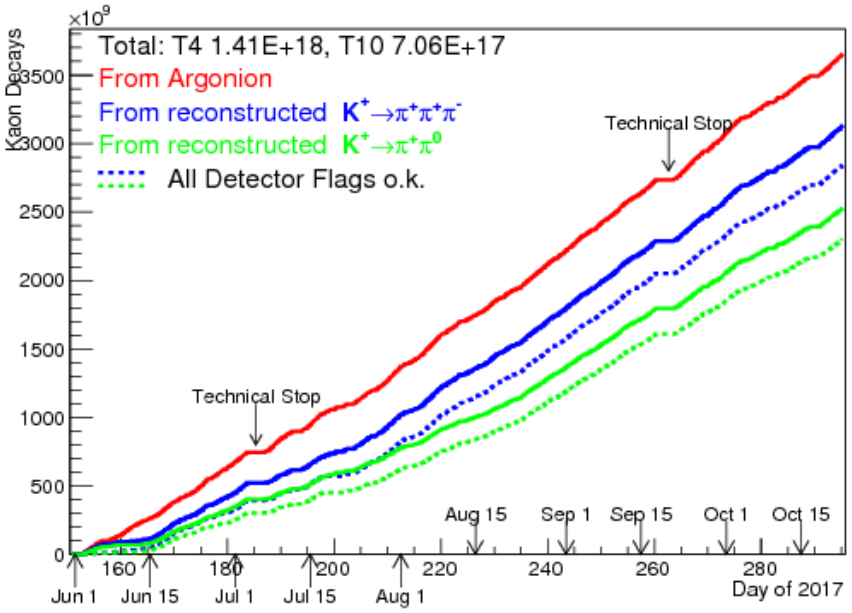

Figure 2: Integrated number of Kaon decays for the 2017 data-taking as a function of time. Red: Delivered (measured by an ionization chamber at the end of the K12 beam). Blue, green: registered Kaon decays obtained using $K^+ \to \pi^+\pi^+\pi^-$ and $K^+ \to \pi^+\pi^0$ decays. Dashed: same, but all detectors functioning correctly. Effects due to random veto (more prominent in the used $K^+ \to \pi^+\pi^0$ selection) are not taken into account.

to fully exploit our allocated quota, we reduced the memory usage of the reconstruction and analysis programs to below 2GByte. This total overhaul of the production system lead to a reduction in processing time for larger data-sets by nearly a factor 10. We can now process data about a factor of four faster than we collect them: a data set from one month of data taking can be processed within one week.

Another major improvement was the development of sub-detector and trigger monitoring tools in order to automatically assess each single SPS spill based on the sub-system performances, to discard for physics analysis the ones in which any anomalous response was observed. From such a detailed study of the detector performances, several new hardware or firmware problems were identified, and procedures to correct them during the offline data processing were developed. For instance, one of the identified problems is the occasional "swap" of the first and second group of 16 channels within a 32-channel CREAM module, which leads to a temporary misconfiguration of the channel mapping. This issue, which is due to an instability in the part of the CREAM firmware managing the board initialization, is now corrected during the offline processing on a burst basis, by detecting and inverting the affected channels in the reconstruction software. Furthermore, in order to fine-tune the detector time alignment (in particular of KTAG and RICH, which have a time resolution of 70 ps) we also determine the time offsets on a per burst basis to be used in the data reconstruction; this was particularly important for data towards the end of the 2017 data taking, when hardware issues caused time drifts of up to 1 ns in few hours. With this improved calibration procedure, the detector time alignment is restored and the residual jitter due to the time drifts is less than 10 ps.

All the new procedures developed for the offline processing have been added to the online

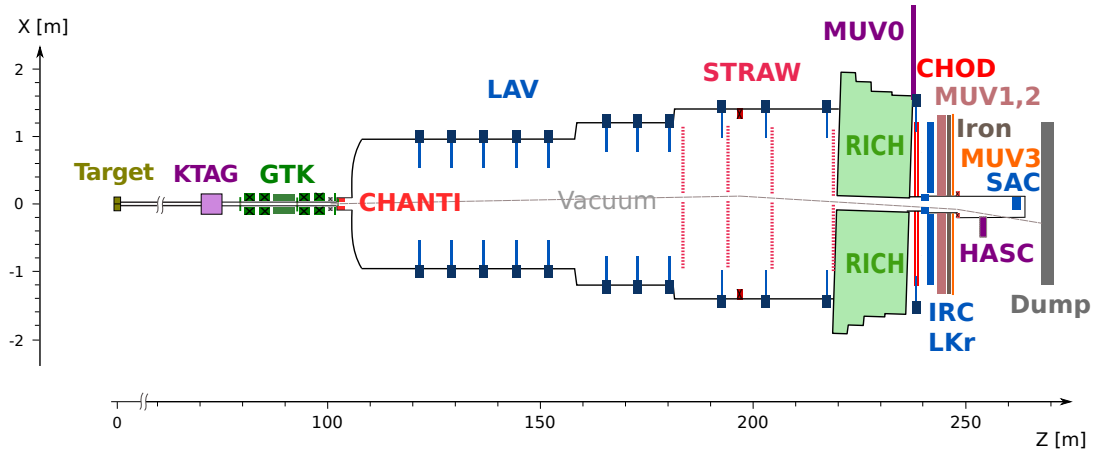

Figure 3: Layout of the NA62 experiment. KTAG: Cerenkov threshold counter; GTK: Si pixel beam tracker; CHANTI: ring stations of scintillator slabs; LAV: lead glass ring calorimeters; STRAW: straw magnetic spectrometer; RICH: ring imaging Cerenkov counter; MUV0: off-acceptance plane of scintillator pads; CHOD: planes of scintillator pads and slabs; IRC: inner ring shashlik calorimeter; LKr: electromagnetic calorimeter filled with liquid krypton; MUV1,2: hadron calorimeter; MUV3: plane of scintillator pads for muon veto; HASC: near beam lead–scintillator calorimeter; SAC: small angle shashlik calorimeter.

data quality monitoring system, and they will be used during the 2018 data taking, thanks also to the installation of additional online computing power. Quality checks are performed on three different time scales: hit maps are obtained from scalers (implemented electronically in the TEL62 boards) for every burst and displayed for the shift crew within 15 s after the burst was written to disk; full reconstruction is ran over one in thirty events and hit maps, energy reconstructions, time resolutions, etc are displayed within 3 minutes. At this step, also checks for known hardware problems (like the before mentioned "swaps") are performed and messages are sent to the shift crew. Finally, on the timescale of one day, most runs are fully reconstructed and a physics analysis is performed to measure in particular the π^0 and μ^+ rejection for the $K^+ \to \pi^+\nu\bar{\nu}$ analysis.

4 $K^+ \to \pi^+\nu\bar{\nu}$ Analysis

The first $K^+ \to \pi^+\nu\bar{\nu}$ analysis (later noted as $\pi\nu\nu$) has been performed on a sample of data taken from mid-September to mid-October 2016. This is the first set of data declared good for $\pi\nu\nu$. It has been acquired at an average intensity of 35–40% of the nominal one. In 2016 the spill structure of the SPS beam was irregular, with intensity spikes causing NA62 to sustain running conditions even above nominal intensity and lasting for several ms. Beam fluctuations have been reduced in 2017, making possible to run at an average intensity of 60–65%.

The description of the $\pi\nu\nu$ analysis given below makes use of acronyms to indicate the NA62 sub-detectors, following the conventional naming scheme shown in Figure 3. A detailed description of the NA62 detector can be found in [1].

Data for $\pi\nu\nu$ have been collected with a two-level trigger stream (PNN). A hardware-based trigger (L0) used RICH, CHOD, LKr and MUV3 to veto μ^+ and γ while keeping π^+. A software-based trigger (L1) exploited K^+ identification with KTAG, γ rejection with LAV and

track reconstruction with STRAW. The analysis made also use of data taken with a downscaled minimum-bias trigger (control trigger) to compute the K^+ flux and to select control samples.

Data collected in 2016 for $\pi\nu\nu$ have been reprocessed in 2017 using the final sets of detector calibrations in the reconstruction step and then filtered to produce a dedicated $\pi\nu\nu$ stream for analysis. Because of hardware problems affecting data in 2016, mainly due to HV problems due to a krypton leak, only 50k bursts have been declared good for data analysis, about 35% less than expected. This problem does not affect 2017 data for which the rate of bad quality bursts is below percent.

A blind procedure was adopted for the 2016 $\pi\nu\nu$ analysis, with signal and control regions kept masked as long as the evaluation of expected signal and background was not complete. The un-blinding took place in March 2018 and the preliminary result presented at the Moriond EW conference [2] and in a dedicated seminar at CERN [3]. To be consistent with the blind analysis procedure, only minor changes are allowed for the final result. That will appear in a physics paper in preparation.

The $\pi\nu\nu$ analysis of 2016 data is mostly cut-based. The branching ratio of $K^+ \to \pi^+\nu\bar{\nu}$ predicted by the SM is $BR(K^+ \to \pi^+\nu\bar{\nu}) = (0.84 \pm 0.10) \times 10^{-10}$ [4]. The goal of the analysis is to demonstrate the background reduction capabilities of NA62 down to the SM sensitivity. The analysis is organized into: selection, evaluation of the single event sensitivity, background estimation and validation, un-blinding of signal regions and interpretation of the results. Specifically selected control samples of $K^+ \to \pi^+\pi^0(\gamma)$, $K^+ \to \mu^+\nu(\gamma)$ and $K^+ \to \pi^+\pi^+\pi^-$ are employed for background studies.

4.1 $K^+ \to \pi^+\nu\bar{\nu}$ Selection

The $\pi\nu\nu$ selection proceeds through: definition of a K^+ decay with a charged particle in the final state; π^+ identification; rejection of events with γ or any other activity in final state; kinematic selection and definition of the signal regions. In order to keep performances suitable for $\pi\nu\nu$, essential actions are taken during the run and at reprocessing stage: KTAG alignment and pressure scan; RICH mirrors alignment; GTK and STRAW geometrical alignment; GTK time alignment; LKr energy calibration; global and burst-dependent relative time alignment of all the detectors.

The selection starts reconstructing the π^+ and its parent K^+. RICH, CHOD and LKr signals are spatially associated to each good–quality track reconstructed in the STRAW and timestamp the π^+ with $\mathcal{O}(100$ ps) resolution. Consistency between π^+ and trigger time defines a single charged particle event topology. A K^+ is identified in KTAG and traced in GTK. The parent K^+ is matched to the π^+ exploiting the $\mathcal{O}(100$ ps) time coincidence resolution between KTAG, GTK and RICH and the $\mathcal{O}$(mm) resolution of the closest distance of approach between the STRAW and GTK tracks. The K^+ mis-matching probability is $\mathcal{O}(\%)$, depending linearly on the instantaneous beam intensity; the K^+ identification efficiency about 75%. The fiducial decay region for $\pi\nu\nu$ starts from 5-10 m downstream of the last GTK station and ends 15 m upstream of the first STRAW chamber. Selection of K^+ decays in this region requires rejection of π^+ coming from K^+ decay along the beam line or produced via interactions of beam particles with the GTK material. This is achieved using criteria based on: reconstructed decay vertex, π^+ position extrapolated back at the entrance of the fiducial region, π^+ emission angle, extra-activity in CHANTI and GTK.

Let p_{K^+} (p_{π^+}) be the K^+ (π^+) 4-momenta measured by the GTK (STRAW), the invariant $m^2_{miss} \equiv (p_{K^+} - p_{\pi^+})^2$ is used to discriminate between the signal and background kinematics. Figure 4 (left) shows the distribution of the selected K^+ decays in the $(m^2_{miss} - P_{\pi^+})$ plane, with P_{π^+} the magnitude of the π^+ 3-momentum. Regions populated mostly by $K^+ \to \pi^+\pi^0(\gamma)$, $K^+ \to \mu^+\nu(\gamma)$ and $K^+ \to \pi^+\pi^+\pi^-$ are visible. Two signal regions are defined: the region at

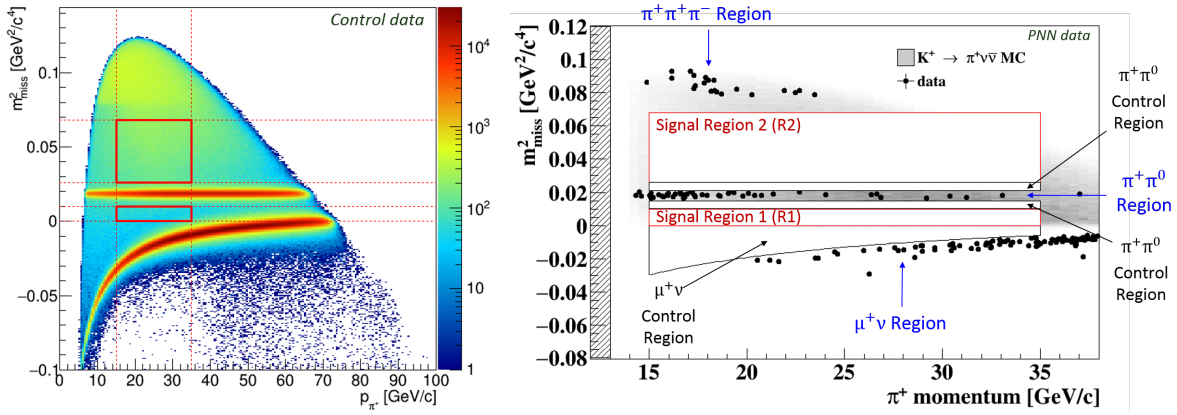

Figure 4: Left: m^2_{miss} as a function of P_{π^+} for control data after K^+ decay selection. Red boxes define the signal regions. Right: m^2_{miss} as a function of P_{π^+} for PNN trigger data events (dots) passing the $\pi\nu\nu$ selection, but the cuts on m^2_{miss} and P_{π^+}. Grey area corresponds to the distribution of $\pi\nu\nu$ MC events, with darker (lighter) grey indicating more (less) populated regions. Red (black) lines define the signal (control) regions and are masked. Three background regions are also shown.

lower (higher) m^2_{miss} is referred in the text as *region* 1 (2). The m^2_{miss} resolution, quantified as 10^{-3} GeV^2/c^4 for the $K^+ \to \pi^+\pi^0$ peak, drives the choice of the boundaries of these regions. The $\pi\nu\nu$ analysis is restricted to $15 < P_{\pi^+} < 35$ GeV/c. This cut costs half of the signal acceptance, but ensures at least 40 GeV/c of missing energy, improving significantly the π^0 detection.

Calorimeters and RICH provide π^+ identification. A multi-variate classifier combines LKr, MUV1 and MUV2 information related to the energy associated to the π^+, its energy–deposition shape and sharing. RICH variables are combined to build: a STRAW track-based likelihood discriminant; the mass of the particle using the momentum measured by the STRAW; the momentum of the particle assuming the π^+ mass. Achieved performances for π^+ momentum between 15 and 35 GeV/c are: 0.6×10^{-5} μ^+ versus 78% π^+ efficiency with calorimeters, 2.1×10^{-3} μ^+ versus 82% π^+ efficiency with RICH.

The LAV, LKr, IRC and SAC ensure rejection of photons with direction from 0 up to 50 mrad with respect to the beam axis. The time coincidence between extra energy in these detectors and π^+ is the main veto condition. Time–energy correlation is exploited in LKr to reduce signal random losses due to accidental activity. Typical veto time windows range from ± 3 to ± 10 ns. Further selection criteria, called multiplicity rejection, are employed against photons interacting with material upstream of photon vetoes and losing energy either in the beam pipe or through hadron production. Multiplicity rejection involves detection of: extra activity in CHOD in coincidence with LKr energy deposits; extra segments reconstructed in STRAW; signals in the off-acceptance detectors HASC and MUV0. Multiplicity rejection is also effective against decays like $K^+ \to \pi^+\pi^+\pi^-$ and $K^+ \to \pi^+\pi^- e^+\nu$. The achieved π^0 detection inefficiency is about 2.5×10^{-8}. This is measured directly on data comparing control trigger and PNN trigger candidates in the $\pi^+\pi^0$ region, passing the $\pi\nu\nu$ selection, before and after γ plus multiplicity rejection, respectively. Alternatively the single photon detection efficiency is measured on data separately for LAV, LKR, IRC and SAC. The corresponding π^0 detection inefficiency is estimated by the convolution of the measured single photon efficiencies with a $K^+ \to \pi^+\pi^0(\gamma)$ simulation, finding good agreement with the direct measurement.

Figure 4 (right) shows the m^2_{miss} versus P_{π^+} distribution of the events passing the $\pi\nu\nu$ selection, but the cuts on m^2_{miss} and P_{π^+}, with the distribution of simulated $K^+ \to \pi^+\nu\bar{\nu}$ superimposed. Three background regions are indicated herein: $\pi^+\pi^0$, $\mu^+\nu$ and $\pi^+\pi^+\pi^-$. Together with the two signal regions, three control regions are defined to validate the $K^+ \to \pi^+\pi^0(\gamma)$ and $K^+ \to \mu^+\nu(\gamma)$ background estimations. Both signal and control regions are masked.

The squared missing mass m^2_{miss} is also computed taking P_{π^+} measured with the RICH instead of the STRAW or assuming the nominal K^+ momentum and direction instead of the GTK measurements. Constraints on these variables are also applied to define signal regions, providing additional power to suppress background coming from tracks mis-reconstructed in STRAW or GTK.

4.2 $K^+ \to \pi^+\nu\bar{\nu}$ Single Event Sensitivity

The single event sensitivity SES is defined as $1/(N_K \cdot \varepsilon_{\pi\nu\nu})$, where N_K is the number of K^+ decays and $\varepsilon_{\pi\nu\nu}$ is the signal efficiency for the $\pi\nu\nu$ selection. The number N_K is estimated using a sample of $K^+ \to \pi^+\pi^0$ and computed as $(N_{\pi\pi} \cdot D)/(A_{\pi\pi} \cdot BR_{\pi\pi})$. Here $N_{\pi\pi}$ is the number of $K^+ \to \pi^+\pi^0$ decays selected on control data using the same $\pi\nu\nu$ criteria, except the γ, the multiplicity rejection and the cut on m^2_{miss}; $A_{\pi\pi}$ their acceptance estimated to be about 10% using a MC simulation; $BR_{\pi\pi}$ and $D = 400$ are the branching ratio of the $K^+ \to \pi^+\pi^0$ decay and the downscaling factor of the control trigger, respectively. The corresponding number of K^+ decays is:

$$N_K = (1.21 \pm 0.02_{syst}) \times 10^{11}.$$

Discrepancies in data/MC agreement and variation of the measured K^+ flux as a function of P_{π^+} are the main sources of systematic uncertainty. Any source of event loss not accounted for or not precisely reproduced by MC is assumed not relevant to N_K, as it cancels in the signal to normalization ratio entering SES.

The signal efficiency is computed separately in four bins of P_{π^+}, 5 GeV/c wide, as the product of three terms, $(A_{\pi\nu\nu} \cdot \epsilon_{RV} \cdot \epsilon_{trig})$. The signal acceptance $A_{\pi\nu\nu}$ is extracted from MC; ϵ_{RV} is the signal efficiency due to losses resulting from γ and multiplicity rejection induced by the random activity in the detectors; ϵ_{trig} the PNN trigger efficiency. Any other effect inducing signal loss is included in $A_{\pi\nu\nu}$ or cancels in the ratio with $A_{\pi\pi}$ when computing SES.

Signal acceptance as a function of P_{π^+} is shown in Figure 5 (left). The overall acceptance is about 4%. Uncertainty is mainly systematic and comes from the simulation of the signal losses resulting from γ and multiplicity rejection induced by π^+ interactions with the detector material (pion-driven losses).

Trigger efficiency is measured using control data and $K^+ \to \pi^+\pi^0$ control samples. The L0 efficiency is about 90%, weakly dependent on P_{π^+}, with losses due mainly to the LKr and MUV3 veto conditions, while L1 is more than 97% efficient.

Random veto efficiency ϵ_{RV} is estimated on data using a sample of $K^+ \to \mu^+\nu$ candidates and is defined as the ratio of the events selected before and after the γ and multiplicity cuts. Muon-driven losses are corrected for using MC, as $A_{\pi\nu\nu}$ already accounts for pion-driven losses. The final result integrated over P_{π^+} is $\epsilon_{RV} = 0.76 \pm 0.04$, where the uncertainty comes from the correction for muon-driven losses. The random veto efficiency is flat as a function of P_{π^+}, but depends on the instantaneous intensity (Figure 5, right).

The final measured SES and the corresponding number of SM $K^+ \to \pi^+\nu\bar{\nu}$ expected in signal regions 1 and 2 are:

$$SES = (3.15 \pm 0.01_{stat} \pm 0.24_{syst}) \times 10^{-10},$$
$$N^{exp}_{\pi\nu\nu}(SM) = 0.267 \pm 0.001_{stat} \pm 0.020_{syst} \pm 0.032_{ext}.$$

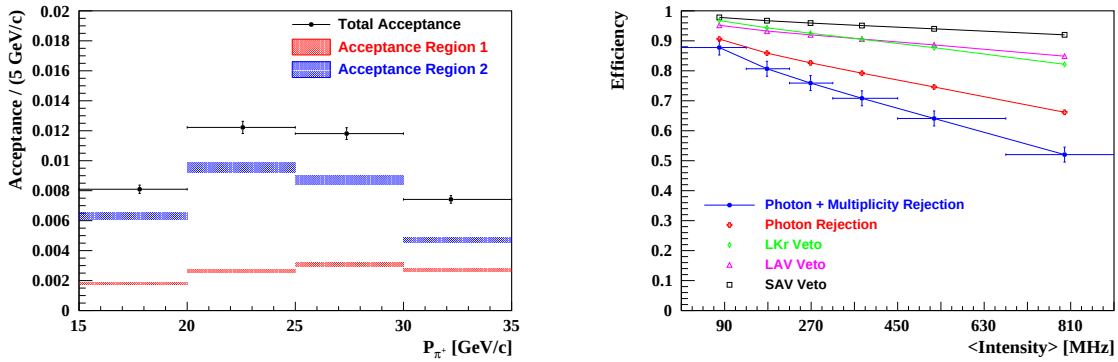

Figure 5: Left: signal acceptance in bins of P_{π^+}. Dots correspond to the acceptance in region 1 plus 2 with statistic and systematic errors summed in quadrature. The horizontal bars indicate the 5 GeV/c bin size. Blue and red boxes are the acceptances in region 1 and 2, respectively. The vertical size of the boxes corresponds to the statistic plus systematic errors. Right: efficiency against random signal losses from γ and multiplicity rejection in bins of instantaneous intensity. The out-of-time activity in GTK is used as estimator of the intensity. Blue dots are the total efficiency with its systematic uncertainty (see text); the horizontal bar indicates the width of the bin. Red crosses represent the efficiency after γ rejection; vertical and horizontal bars are omitted. The effect of the multiplicity rejection on ϵ_{RV} is given by the difference between red crosses and blue dots. The other symbols illustrate the effect on ϵ_{RV} of IRC and SAC only (black square), LAV only (pink triangle), LKr only (green diamond). Lines are for eye guidance only.

The external error to $N_{exp}^{\pi\nu\nu}(SM)$ comes from the uncertainty on the SM $\pi\nu\nu$ branching ratio. The systematic uncertainty on SES mostly comes from ϵ_{RV} and $A_{\pi\pi}$ and is propagated to $N_{\pi\nu\nu}^{exp}$.

4.3 Background Studies

Background from K^+ decaying in the fiducial region comes primarily from $K^+ \to \pi^+\pi^0(\gamma)$, $K^+ \to \mu^+\nu(\gamma)$, $K^+ \to \pi^+\pi^+\pi^-$ and $K^+ \to \pi^+\pi^-e^+\nu$.

The m^2_{miss} spectrum of $K^+ \to \pi^+\pi^0(\gamma)$, $K^+ \to \mu^+\nu(\gamma)$ and $K^+ \to \pi^+\pi^+\pi^-$ is limited by well defined kinematic thresholds. To estimate the background from these decays entering signal regions, the assumption is made that π^0 rejection for $K^+ \to \pi^+\pi^0(\gamma)$, particle identification for $K^+ \to \mu^+\nu(\gamma)$ and multiplicity rejection for $K^+ \to \pi^+\pi^+\pi^-$ are independent from the cuts on m^2_{miss} defining the signal regions. The number of expected events in signal regions from these processes, $N^{exp}_{background}$, is computed as $N(background) \cdot f^{kin}$; here $N(background)$ is the number of remaining PNN triggered events in the corresponding background region after the $\pi\nu\nu$ selection, but the cut on m^2_{miss} (Figure 4, right); f^{kin} is the fraction of background events entering signal regions through the reconstructed tails of the corresponding m^2_{miss} peak. The fraction f^{kin}, called *tails*, is modeled on control samples selected on data and eventually corrected for biases induced by the selection criteria using MC simulations. The above procedure is applied separately in four bins of P_{π^+} for $K^+ \to \pi^+\pi^0(\gamma)$ and $K^+ \to \mu^+\nu(\gamma)$. Expected background in control regions is derived similarly.

The reconstruction tails of the $K^+ \to \pi^+\pi^0(\gamma)$ m^2_{miss} distribution are studied from a $K^+ \to \pi^+\pi^0(\gamma)$ control sample selected tagging the π^0 with two γ's in LKr. Simulation accurately reproduces the tails over 4–5 orders of magnitudes (Figure 6, left). The π^0 tagging does

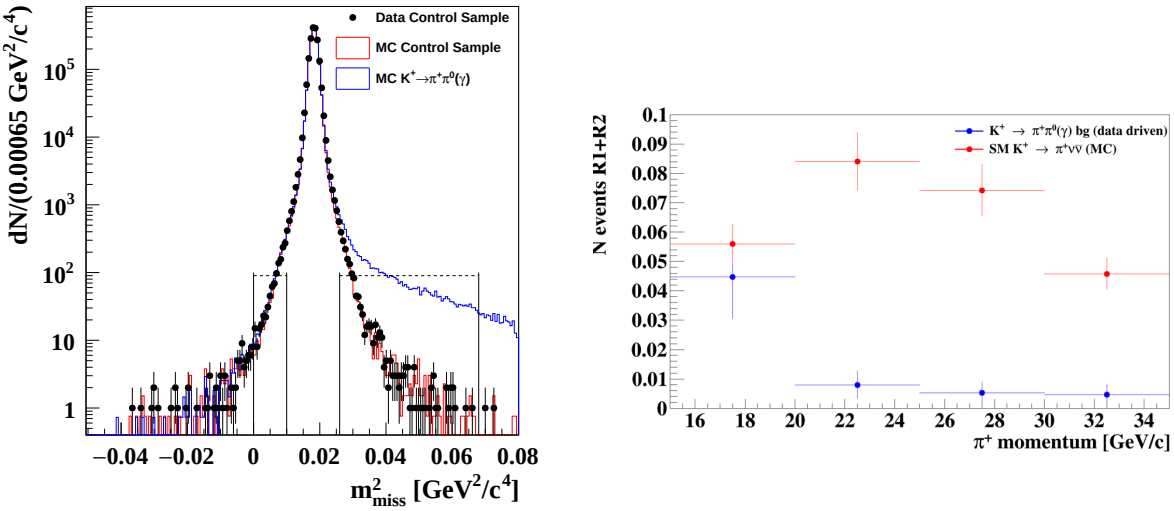

Figure 6: Left: m^2_{miss} distribution of the $K^+ \to \pi^+\pi^0(\gamma)$ control events selected on data tagging the π^0 (dots). Two $K^+ \to \pi^+\pi^0(\gamma)$ MC samples are superimposed: one selected as in data (red line), the other selected as $\pi\nu\nu$ (blue line, referred as MC $K^+ \to \pi^+\pi^0(\gamma)$ in the legend). The region between the two vertical lines joined by the dotted horizontal line at m^2_{miss} lower (higher) than the $m^2_{\pi^0}$ peak indicates region 1 (2). Right: expected $K^+ \to \pi^+\pi^0(\gamma)$ background in bins of P_{π^+} compared to the expected number of SM $K^+ \to \pi^+\nu\bar{\nu}$ events.

not bias the resolution tails of $K^+ \to \pi^+\pi^0(\gamma)$, but suppresses almost completely the radiative part. This is evident comparing m^2_{miss} of control sample events and $K^+ \to \pi^+\pi^0(\gamma)$ MC events selected as $\pi\nu\nu$ without applying γ and multiplicity rejection (blue curve in Figure 6, left). The contribution of the radiative decay to the $K^+ \to \pi^+\pi^0(\gamma)$ background is estimated separately: the photon–veto rejection factor of radiative decays entering region 2 is derived from the measured single photon detection efficiency and applied to each of the three photons in the final state of the simulated $K^+ \to \pi^+\pi^0\gamma$ events. The $K^+ \to \pi^+\pi^0(\gamma)$ expected background summed up in bins of P_{π^+} is summarised in Table 1. The radiative part accounts for about 13% of the total background and dominates the systematic uncertainty. The background depends on P_{π^+} as residual PNN trigger events in $\pi^+\pi^0$ region gather at low P_{π^+} (Figure 6, right). After un-blinding the $K^+ \to \pi^+\pi^0(\gamma)$ control regions, one event is observed while $1.46 \pm 0.16_{stat} \pm 0.06_{syst}$ are expected.

Reconstruction tails of $K^+ \to \mu^+\nu(\gamma)$ are modeled by a control sample selected tagging μ^+ in MUV3. Like $K^+ \to \pi^+\pi^0(\gamma)$, comparison between data and MC suggests that tails are accurately simulated over 5 orders of magnitude (Figure 7, left). The bias induced by the selection of the control sample is assigned as systematic uncertainty. Unlike $K^+ \to \pi^+\pi^0(\gamma)$, the radiative contribution is included in the measured tails. RICH potentially correlates particle identification and kinematics if $K^+ \to \mu^+\nu$ events enter signal regions because of P_{π^+} mis-measurement in STRAW. The effect on background is estimated on data comparing RICH performances measured on $K^+ \to \mu^+\nu(\gamma)$ events in $\mu^+\nu$ and signal regions. Performances are found compatible in the two cases and the statistical uncertainty is assigned as systematic error. The expected $K^+ \to \mu^+\nu(\gamma)$ background summed up in bins of P_{π^+} is summarised in Table 1. The background depends on P_{π^+} as both tails and particle identification steeply increase at higher

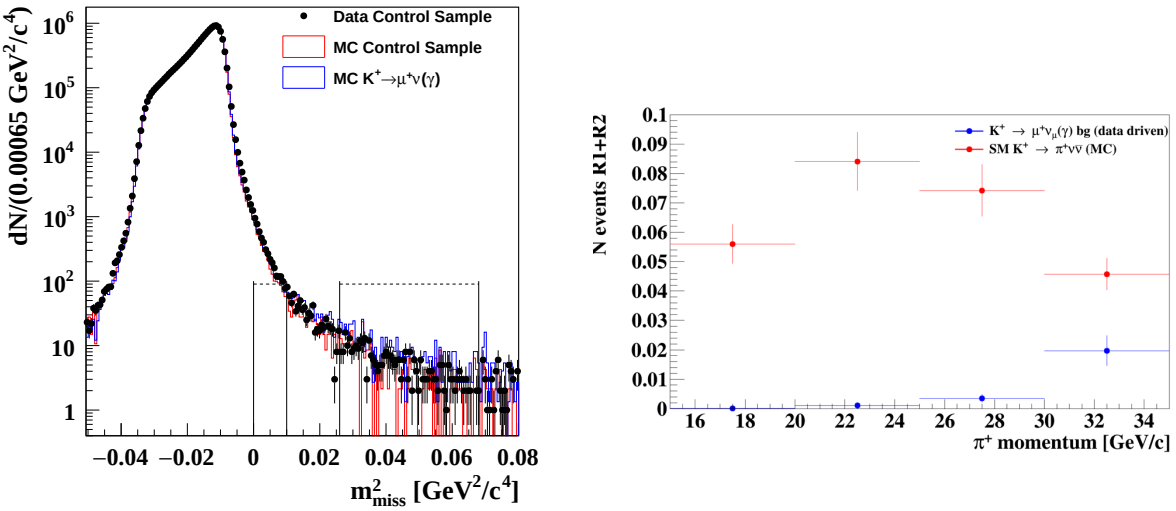

Figure 7: Left: m^2_{miss} distribution of the $K^+ \to \mu^+\nu(\gamma)$ control events selected on data (dots) with two MC $K^+ \to \mu^+\nu(\gamma)$ samples superimposed: one selected as in data (red line), the other selected as $\pi\nu\nu$ without particle identification (blue line, referred as MC $K^+ \to \mu^+\nu(\gamma)$ in the legend). The two regions between the two vertical lines joined by the dotted horizontal line correspond to region 1 and 2 (lower and higher m^2_{miss}, respectively). Right: expected $K^+ \to \mu^+\nu(\gamma)$ background in bins of P_{π^+} compared to the expected number of SM $K^+ \to \pi^+\nu\bar{\nu}$ events.

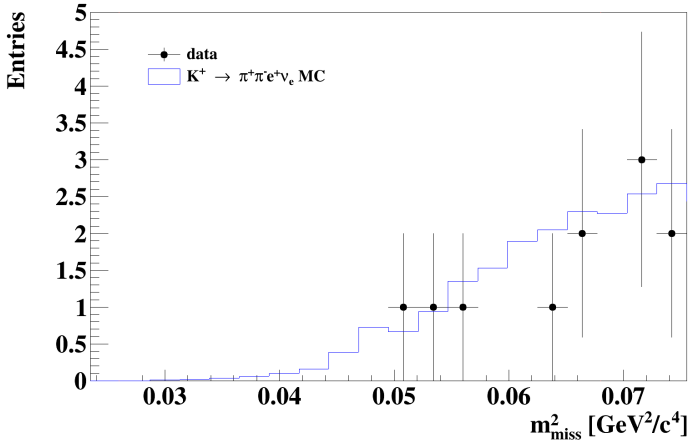

Figure 8: Data and MC distributions of m^2_{miss} for a K_{e4}-enriched validation sample. Data and MC agree within statistical uncertainty.

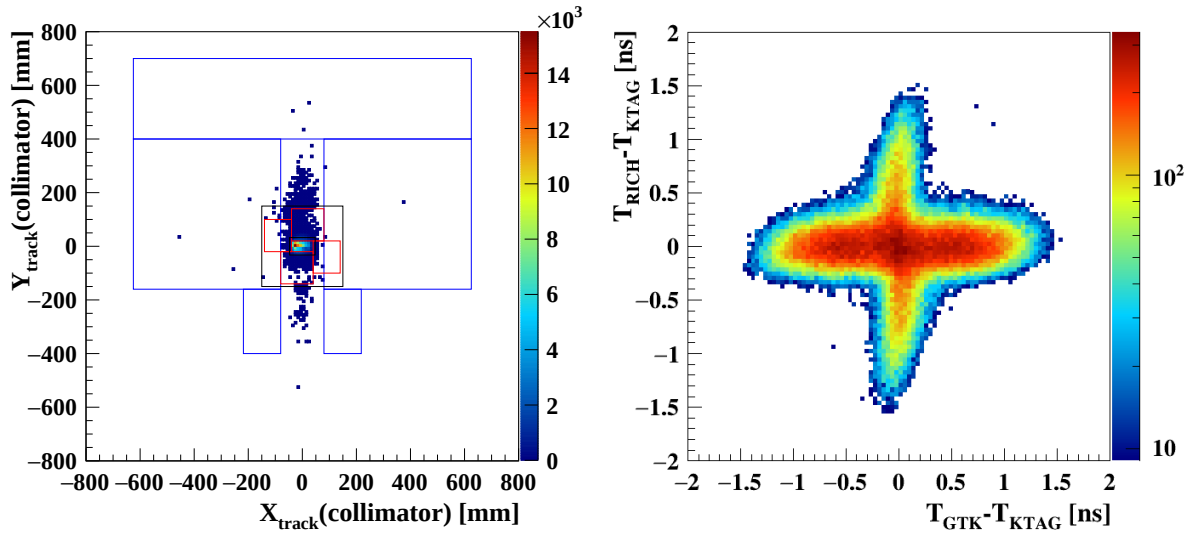

Figure 9: Left: position at Trim5 of π^+'s from a data sample enriched for upstream events. Blue lines correspond to the contour of the last dipole of the second achromat; red lines show the contour of the final collimator; black line indicate the acceptance region covered by CHANTI. Right: time difference between RICH and KTAG versus GTK and KTAG for the same π^+'s of the left plot.

momenta as a consequence of $K^+ \to \mu^+\nu$ kinematics and RICH performances, respectively (Figure 7, right). After un-blinding the $K^+ \to \mu^+\nu(\gamma)$ control region, two events are observed while $1.02 \pm 0.16_{stat}$ are expected.

The $K^+ \to \pi^+\pi^+\pi^-$ decays could enter primarily region 2. The expected background is evaluated using a method similar to $K^+ \to \pi^+\pi^0(\gamma)$ and $K^+ \to \mu^+\nu(\gamma)$. Multiplicity rejection and kinematic cuts turn out to be very effective against $K^+ \to \pi^+\pi^+\pi^-$ decays and the expected background is found to be an order of magnitude lower than $K^+ \to \mu^+\nu(\gamma)$ (Table 1).

Background from $K^+ \to \pi^+\pi^-e^+\nu$ (K_{e4}) is expected in signal region 2. It is suppressed by multiplicity rejection, particle identification, kinematics and by the branching ratio of 4.25×10^{-5} [5]. However the factorization approach used to determine the expected background from $K^+ \to \pi^+\pi^0(\gamma)$, $K^+ \to \mu^+\nu(\gamma)$ and $K^+ \to \pi^+\pi^+\pi^-$ does not apply to K_{e4}, as kinematics is strongly correlated to topology. Background from K_{e4} is therefore estimated via simulation. A MC sample of $4{\times}10^8$ K_{e4} decays is employed and validated on data using different K_{e4} enriched selections, orthogonal to $\pi\nu\nu$ (Figure 8). After the full $\pi\nu\nu$ selection two K_{e4} events remain. The corresponding expected background is summarised in Table 1. The statistics of the MC sample is the limiting factor of the final estimation.

Considerations based on selection performances (Section 4) show that background from $K^+ \to e^+\pi^0\nu$ or $K^+ \to \mu^+\pi^0\nu$ decays is negligible. Simple simulations show that kinematics and branching ratio make backgrounds from rare decays like $K^+ \to \pi^+\gamma\gamma$ negligible.

In addition to K^+ decays in the fiducial region, backgrounds can originate from upstream events classified as:

1. π^+ from K^+ decays upstream of the decay region, most notably between GTK stations 2 and 3, matched to a pileup beam particle;

2. π^+ from interactions of a beam π^+ mostly with GTK station 3, but also with station 2, matched to a pileup K^+;

3. π^+ from interactions of a K^+ with material in the beam, produced either as prompt particle originating from the interaction or as a decay product of a neutral kaon.

The interpretation of the upstream events in terms of the above topologies is supported by a closer look to a $\pi\nu\nu$-like data sample enriched for upstream events. The position of the π^+ mesons at the entrance of the decay region (Trim5) (Figure 9, left) indicates their origin upstream or via interactions in GTK stations and drives the choice of a geometrical cut covering the central aperture of the dipole (box cut defined by $|X_{track}| < 100$ mm and $|Y_{track}| < 500$ mm); the distribution of the time coincidence between KTAG-RICH and GTK-KTAG suggests an accidental source for these events (Figure 9, right). The estimation of the upstream background is made on data using a bifurcation technique. The $K^+ - \pi^+$ matching and the box cut are chosen to be the selection criteria to invert, called $cut1$ and $cut2$, respectively. The combination of $cut1$ and $cut2$ defines four samples, noted A, B, C and D: A is the signal and D is the sample with both criteria inverted. The expected events in A correspond to $B \cdot C/D$ if all the samples contain the same type of events and $cut1$ and $cut2$ are independent. To verify this independence, the selection conditions are relaxed simultaneously to create disconnected samples in the $(cut1, cut2)$ plane. For each set of disconnected samples the method is validated testing the stability of the prediction in region A and comparing expectations and observations in control regions of the $(cut1, cut2)$ plane. Five sets of selection criteria are employed by the $\pi\nu\nu$ analysis, all of them validating the upstream background estimation within their statistical precision. The expected upstream background is shown in Table 1. The statistics of the bifurcated samples limits the accuracy of the final value.

Process	Expected events in signal regions
$K^+ \to \pi^+\pi^0(\gamma)$ IB	$0.064 \pm 0.007_{stat} \pm 0.006_{syst}$
$K^+ \to \mu^+\nu(\gamma)$ IB	$0.020 \pm 0.003_{stat} \pm 0.003_{syst}$
$K^+ \to \pi^+\pi^- e^+\nu$	$0.018^{+0.024}_{-0.017}\vert_{stat} \pm 0.009_{syst}$
$K^+ \to \pi^+\pi^+\pi^-$	$0.002 \pm 0.001_{stat} \pm 0.002_{syst}$
Upstream Background	$0.050^{+0.090}_{-0.030}\vert_{stat}$
Total Background	$0.15 \pm 0.09_{stat} \pm 0.01_{syst}$

Table 1: Summary of the background estimation from the $\pi\nu\nu$ analysis of 2016 data.

Table 1 summarizes the final expected background in signal region 1 and 2. In total $0.15 \pm 0.09_{stat} \pm 0.01_{syst}$ background events are expected in region 1 and 2.

4.4 Results

After un-blinding the signal regions, one event is found in region 2, as shown in Figure 10 (left). The corresponding π^+ has a momentum of 15.3 GeV/c. The RICH clearly indicates that it is a pion (Figure 10, right). Table 2 summarizes the final numbers from the $\pi\nu\nu$ analysis of the 2016 data. A preliminary observed upper limit to the branching ratio of the $K^+ \to \pi^+\nu\bar{\nu}$ decay is derived from these results using the CL_s method [6]:

$$BR(K^+ \to \pi^+\nu\bar{\nu}) < 14 \times 10^{-10} \text{ @ } 95\% \ CL.$$

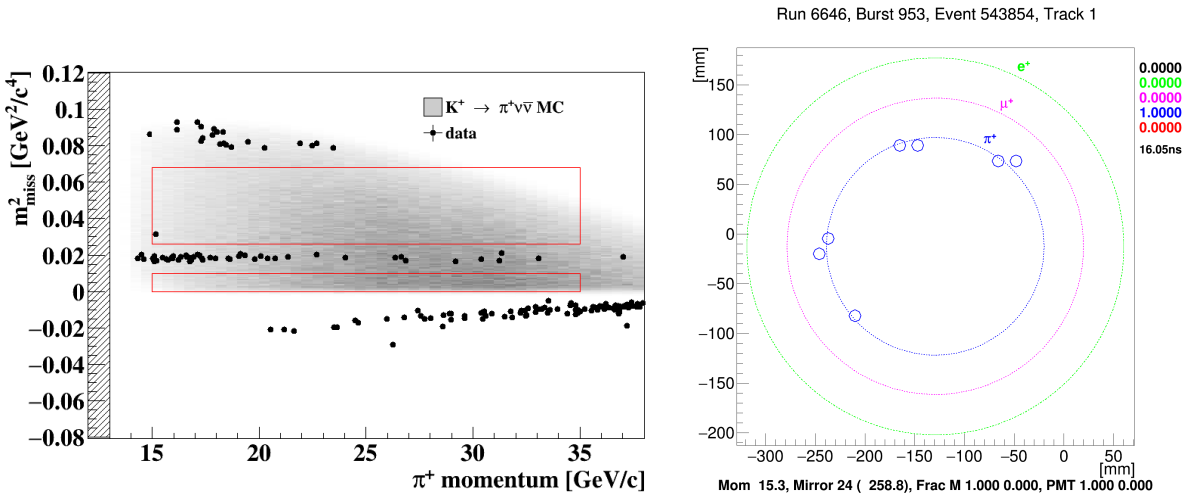

Figure 10: Left: m^2_{miss} as a function of P_{π^+} for PNN trigger data events (dots) passing the $\pi\nu\nu$ selection, but the cuts on m^2_{miss} and P_{π^+}. The grey area corresponds to the distribution of $\pi\nu\nu$ MC events. Red lines define the signal regions. The event observed in region 2 is shown. Right: position of the hits in the RICH forming the ring associated to the π^+ of the observed event in region 2, as given by the RICH event display. The circles illustrate the positron, muon and pion hypothesis, showing a perfect agreement of the observed event with the pion hypothesis.

Observed Events	1
SES	$(3.15 \pm 0.01_{stat} \pm 0.24_{syst}) \cdot 10^{-10}$
Expected SM $K^+ \to \pi^+\nu\bar{\nu}$	$0.267 \pm 0.001_{stat} \pm 0.020_{syst} \pm 0.032_{ext}$
Expected Background	$0.15 \pm 0.09_{stat} \pm 0.01_{syst}$

Table 2: Summary of the results from the $\pi\nu\nu$ analysis of 2016 data.

The corresponding expected limit is $BR(K^+ \to \pi^+\nu\bar{\nu}) < 10 \times 10^{-10}$ @ 95% CL. The observed limit derived using a different statistical treatment [7] is found to be in agreement.

4.5 Summary and Prospects

The analysis of the 2016 data shows that the decay-in-flight technique of NA62 to study $K^+ \to \pi^+\nu\bar{\nu}$ works. The acceptance is about 20 times larger than what achieved by the stopping kaon technique [8, 9], such that this result is already competitive (in region 2) with just $\approx$ 1% of the total expected statistics of NA62.

Improvements both at hardware and analysis level are planned to reduce the background and improve signal efficiency. The 2016 analysis has shown that the upstream background is relevant. In order to keep it under control tight geometrical cuts are employed at analysis level causing up to 30–40% signal acceptance reduction. The principal source of upstream background is due to the lack of shielding at the position of the final collimator corresponding to the aperture of the last dipole of the second achromat. Already in the final part of the 2017 data–taking

a copper plug was inserted into the dipole to mitigate this issue. Now that the beam tuning is complete, the replacement of the adjustable final collimator with a fixed one which extends further transversally will improve our immunity to upstream interactions. The installation of this collimator is foreseen in mid June 2018.

Reduction of background and improvement of signal acceptance are also expected by gradually moving the analysis from a cut based to a multi-variate approach. In this respect the discrimination of backgrounds like $K^+ \to \pi^+\pi^0(\gamma)$ and $K^+ \to \mu^+\nu(\gamma)$ from signal will profit also of the shape of relevant variables like m^2_{miss} and π^+ momentum; the use of the shape of the time coincidence and of the closest distance of approach between the π^+ and K^+ tracks will improve the separation between signal and upstream background.

The $\pi\nu\nu$ analysis of the 2017 data has started. Considering the statistics collected in 2017 and expected in 2018, NA62 should be able to observe of the order of 20 SM $K^+ \to \pi^+\nu\bar{\nu}$ events. The analysis of the full data sample collected before LS2 should provide a significant result as input to the update of the European Strategy for Particle Physics and a solid extrapolation to the ultimate NA62 sensitivity achievable after LS2.

5 Rare and forbidden decays

5.1 Trigger and data samples

Measurements of rare K^+ and π^0 decays and searches for decays forbidden in the SM benefit from the unprecedented size of the data sample, the excellent resolution on kinematic variables provided by the thin ($1.8\%X_0$) STRAW and the GTK, and the outstanding particle identification and photon veto capabilities of the NA62 detector. However the high beam intensity (requiring complex trigger algorithms, which leads to trigger inefficiencies of typically 10%) and spectrometer design optimized for single-track events represent limiting factors for precision rare decay measurements. Furthermore, geometrical acceptances for certain multi-body rare decays (e.g. $K^+ \to \pi^+\pi^0 e^+e^-$, $K^+ \to \pi^+\gamma e^+e^-$) are below 1% due to the very forward detector geometry.

A number of auxiliary "multi-track" trigger chains designed for collection of K^+ decays to lepton pairs (i.e. di-muons, di-electrons and muon-electron pairs) have been in operation since July 2016. Their L0 (digital electronics) stage is based on RICH and hodoscope hit multiplicity, calorimetric and muon detector information, while their L1 (software) stage involves beam kaon identification by the KTAG and online track reconstruction in the STRAW. Trigger algorithms have been gradually optimized using feedback from online performance studies and physics analysis. The di-muon trigger is typically downscaled by a factor of 2, while the di-electron and muon-electron pair triggers are downscaled by factors up to 10. A generic multi-track trigger chain downscaled typically by a factor 100 is also on operation.

The main $K^+ \to \pi\nu\bar{\nu}$ trigger chain and the minimum bias control trigger based on CHOD signals are also used for a number of rare decay measurements. The latter trigger, unlike all others, is characterized by high efficiency, however it is downscaled by a factor of typically 400.

A number of analyses are in progress based on a partial data sample comprising 50% of the 2016 data and 25% of the 2017 data. Their status is discussed below. The numbers of K^+ decays in the 75 m long fiducial decay volume (FV) quoted below differ between the analyses as a consequence of different downscaling factors applied to the trigger chains.

5.2 Three-track decays

The status of a search for the lepton number violating (LNV) decay $\boldsymbol{K^+ \to \pi^+ e^+ e^-}$ with a data sample corresponding to 1.3×10^{11} kaon decays in FV is summarized in Fig. 11. A

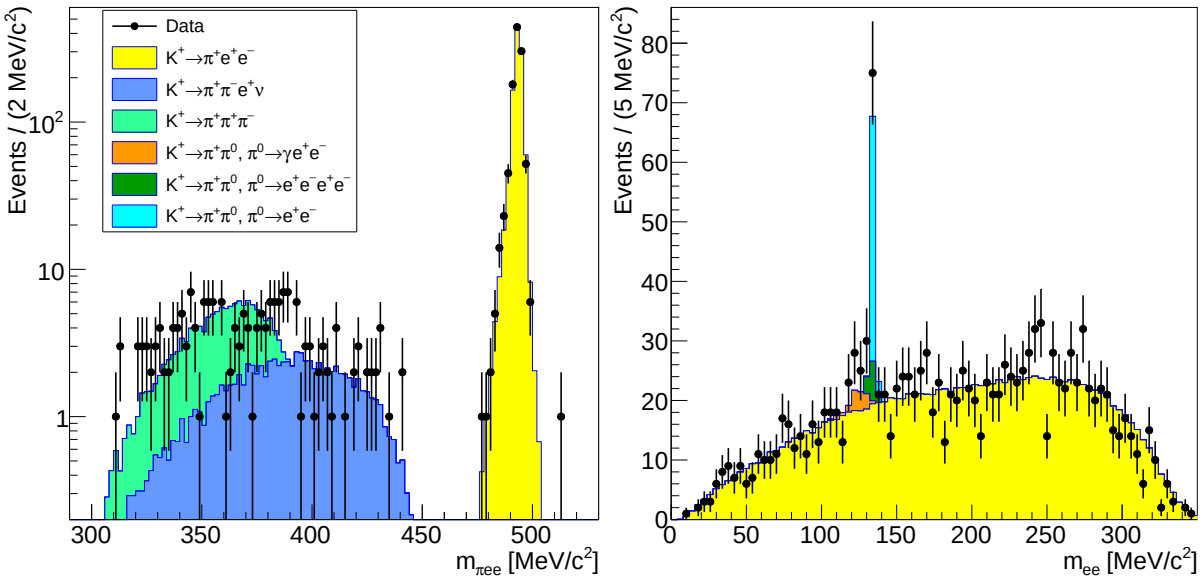

Figure 11: Reconstructed spectra of $K^+ \to \pi^+e^+e^-$ candidates: data (50% of the 2016 sample and 25% of the 2017 sample) and MC estimates of contributions from various processes. Left: $\pi^+e^+e^-$ mass distribution of candidates in the background-free region $m_{ee} > 140$ MeV/c^2. Right: e^+e^- mass distribution of candidates with 488 MeV/c^2 $< m_{\pi ee} <$ 500 MeV/c^2. The $K^+ \to \pi^+e^+e^-$ decay is observed for the first time in the e^+e^- mass range below the π^0 mass, and the rare decay $\pi^0 \to e^+e^-$ is observed.

background-free $K^+ \to \pi^+e^+e^-$ signal of 1.1×10^3 events is observed in the e^+e^- mass region $m_{ee} > 140$ MeV/c^2 (to be compared to the world's largest samples of 0.7×10^4 and 1.0×10^4 candidates [10, 11]), with a $\pi^+e^+e^-$ mass resolution of 1.7 MeV/c^2 and a e^+e^- mass resolution of $\delta(m_{ee})/m_{ee} = 0.004$. The $K^+ \to \pi^+e^+e^-$ process is observed for the first time in the kinematic region $m_{ee} < 140$ MeV/c^2, which is possible due to the suppression of the background from the decay chain $K^+ \to \pi^+\pi^0$, $\pi^0_D \to \gamma e^+e^-$ by the photon veto system. This leads to $\mathcal{O}(10^{-9})$ sensitivity to the branching fraction of the process $K^+ \to \pi^+X$, where X is a new short-lived particle ($\tau_X < 1$ ns) with a mass in the range 10–100 MeV/c^2 decaying mainly into e^+e^-. The rare decay $\pi^0 \to e^+e^-$ (with a branching fraction of 6×10^{-8}) is clearly observed. The search for $K^+ \to \pi^-e^+e^+$ decay is not limited by the background, and the single event sensitivity to the branching ratio of 2×10^{-10} is achieved, improving over the present state of the art [12].

The status of a search for the LNV decay $\boldsymbol{K^+ \to \pi^+\mu^+\mu^-}$ with a data sample corresponding to 6.3×10^{11} kaon decays in FV is summarized in Fig. 12. World's largest $\boldsymbol{K^+ \to \pi^+\mu^+\mu^-}$ sample of 4.6×10^3 candidates is observed, practically with no background and with a $\pi^+\mu^+\mu^-$ mass resolution of 1.2 MeV/c^2. As the most precise $K^+ \to \pi^+\mu^+\mu^-$ measurement to date with 3.1×10^3 candidates is limited by the size of the data sample [13], we expect to produce a competitive $K^+ \to \pi^+\mu^+\mu^-$ measurement with the total NA62 sample of at least 10^4 candidates. The search for the $K^+ \to \pi^-\mu^+\mu^+$ decay is not limited by the background, and the achieved single event sensitivity of 2×10^{-11} improves over the current limit [14]. A search for production and decay of a new light long-lived scalar particle via the process $\boldsymbol{K^+ \to \pi^+S}$, $\boldsymbol{S \to \mu^+\mu^-}$ is also in progress, with a sensitivity to $\mathcal{B}(K^+ \to \pi^+S) \times \mathcal{B}(S \to \mu^+\mu^-)$ of $\mathcal{O}(10^{-10})$ for lifetimes of up to $\mathcal{O}(1$ ns).

Searches for the LNV decay $\boldsymbol{K^+ \to \pi^-\mu^+e^+}$ and the lepton flavour violating (LFV) processes $\boldsymbol{K^+ \to \pi^+\mu^\pm e^\mp}$ with a data sample corresponding to 2.3×10^{11} kaon decays in FV are in progress. The expected backgrounds are different among the three decay modes due to the charge asymmetry of the detector (most importantly, the RICH mirror alignment is optimized

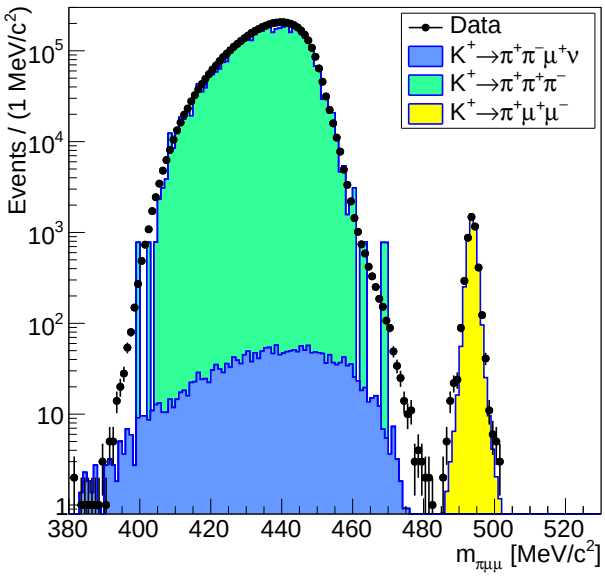

Figure 12: Reconstructed $\pi^+\mu^+\mu^-$ mass spectrum of $K^+ \to \pi^+\mu^+\mu^-$ candidates: data (50% of the 2016 sample and 25% of the 2017 sample) and MC estimates of contributions from potential backgrounds. The description of the tails of the $K^+ \to \pi^+\pi^+\pi^-$ contribution (originating from pion decays in the spectrometer) is limited by simulated statistics; however data and MC agree within statistical uncertainties.

for identification of positive particles), however none of the searches is limited by background. The single event sensitivities achieved are close to 10^{-10} in all cases, improving over the current limits for the $K^+ \to \pi^-\mu^+e^+$ and $K^+ \to \pi^+\mu^-e^+$ modes [12] but not in the $K^+ \to \pi^+\mu^+e^-$ case [15]. Single event sensitivities achieved for the $\boldsymbol{\pi^0 \to \mu^\pm e^\mp}$ decays (with the neutral pions produced in the $K^+ \to \pi^+\pi^0$ process) are 5×10^{-10}, and the signal region is practically background-free due to the additional π^0 mass constraint. We expect to improve on the present limits for these decays [5] using the entire 2016–18 data set.

5.3 One-track decays

A lepton universality test [16] by measurement of $\boldsymbol{R_K = \Gamma(K^+ \to e^+\nu)/\Gamma(K^+ \to \mu^+\nu)}$ is in progress with a partial 2017 data set collected with the main $K^+ \to \pi\nu\bar{\nu}$ trigger chain, which has high efficiency for single positrons with momenta below 30 GeV/c. A novel measurement method proposed is based on the analysis of the reconstructed squared missing mass spectrum: $m^2_{\rm miss} = (p_K - p_e)^2$, where p_K is the kaon 4-momentum measured by the GTK, and p_e is the positron 4-momentum measured by the STRAW. The $m^2_{\rm miss}$ spectrum is presented in Fig. 13: $K^+ \to e^+\nu$ decays are well separated from the $K^+ \to \mu^+\nu$ decays followed by muon decay in flight $\mu^+ \to e^+\nu\bar{\nu}$, and the ratio of event counts for the two components provides a measurement of R_K after corrections for acceptance and backgrounds. The data set analyzed (corresponding to 3×10^{11} kaon decays in FV) contains the world's largest sample of 4×10^5 $K^+ \to e^+\nu$ candidates, and a sample of 6.5×10^6 $K^+ \to \mu^+\nu$ candidates with muon decays in flight. The on-going R_K measurement is not affected by systematic uncertainties (including the one due to $K^+ \to \mu^+\nu$ background with mis-identified muons in the $K^+ \to e^+\nu$ sample) that limited the previous measurement based on the 2007 NA62 data sample [17] thanks to a different measurement technique used.

The same data sample (with a differently optimized event selection) is used to search for heavy neutral lepton (HNL) production in two-body decays $\boldsymbol{K^+ \to e^+N}$ characterized by narrow spikes in the reconstructed missing mass spectrum at large masses. Similarly, a sample

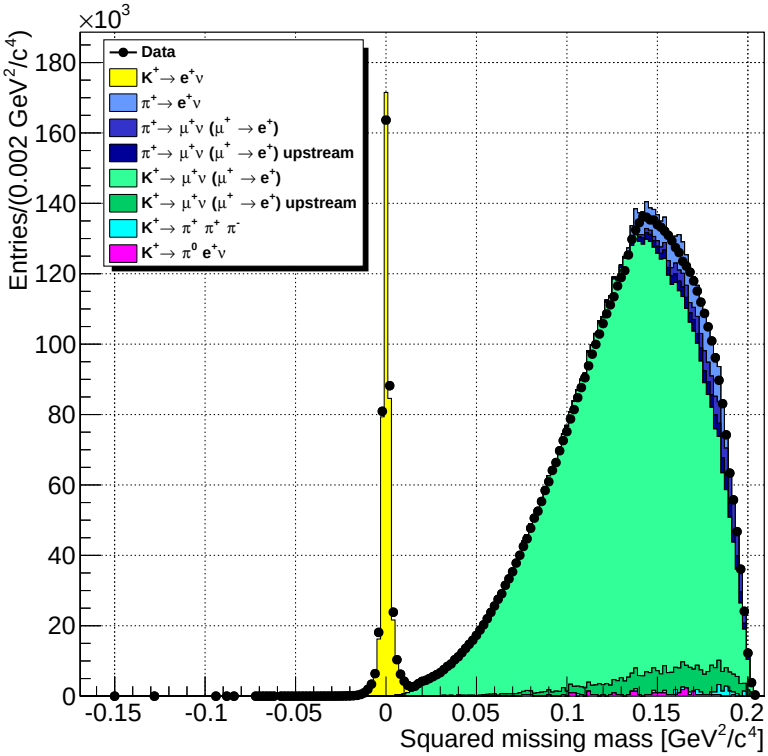

Figure 13: Squared missing mass $m^2_{\text{miss}} = (p_K - p_e)^2$ spectrum used for the R_K measurement and search for heavy neutral lepton production: data and simulated signal and background components. Data correspond to about 30% of the 2017 statistics.

collected with the control trigger (corresponding to 6×10^8 kaon decays in FV) is used to search for HNL production in the process $\boldsymbol{K^+ \to \mu^+ N}$. The unprecedented sensitivity of these searches is underpinned by the excellent background suppression capabilities of the NA62 detector. The recently published results [18] of a pilot HNL production search with a minimum bias sample collected by NA62 in five days of operation at $\mathcal{O}(1\%)$ of nominal beam intensity in 2015 have already improved on the state-of-the-art. Further improvement in sensitivity to the HNL coupling parameters by about two orders of magnitude is expected with the full data set. A search for the $\boldsymbol{K^+ \to e^+ \nu\nu\bar{\nu}}$ decays is also in progress.

Finally, world's largest samples of $\boldsymbol{K^+ \to e^+ \nu\gamma}$ (structure-dependent radiation) and $\boldsymbol{K^+ \to \pi^+ \gamma\gamma}$ decays collected with the control trigger are being analyzed with the aim of measuring the decay spectra and rates.

6 Exotic physics at NA62

Thanks to its high intensity beam and detector performance (redundant particle-identification capability, extremely efficient veto system and high resolution measurements of momentum, time, and energy), NA62 can achieve sensitivities to light mediators in a variety of "exotics" new-physics scenarios. Long-lived mediators weakly coupled to the SM fields can be produced in proton interactions with material along the beam line and can reach the decay volume where they decay. If charged particles are produced as decay products, as is the case for dark photons and heavy neutral leptons, the standard signature would be the identification of a decay vertex from two oppositely charged tracks, spatially displaced from the beam line, and (for two body modes) reconstructing the mass of the new mediator. If photons are produced, as is the case for axion-like particles (ALPs), the signature consists in the reconstruction of two photon clusters in the LKr in absence of charged particle activity, with a peculiar distribution of the total energy and photon-photon barycenter position, resembling the dynamics of the ALP emission.

Such scenarios are under test using two different samples recorded both in 2016 and 2017: one small sample has been recorded without the beryllium target and with the proton beam dumped on the closed movable beam-definig collimator (TAX), almost 20 m downstream the target; the other one was recorded in parallel to the standard data-taking using dedicated low-bandwith triggers that selects configuration topolgies with pair of tracks in the final state. A summary of the available data statistics, expressed in total number of protons on target (POT) is shown in Table 3.

Configuration	Statistics available, POT	Trigger
Beam dump	9×10^{15}	Two tracks
Beam dump	5.5×10^{15}	> 3 GeV deposited in LKr
Standard	3×10^{17}	Di-muon
Standard	10^{17}	Pion-muon
Standard	5×10^{16}	Di-electron
Standard	5×10^{16}	Electron-pion

Table 3: Summary of data recorded in 2016 and 2017 to be used for searches for long-lived new-physics exotic states.

6.1 Search for long-lived dark photons

A popular dark photon model includes the interactions of a new-physics vector via its kinetic-mixing with the SM electromagnetic field [19]. The coupling ϵ and the dark-photon mass are free parameters. The search for dark photons at NA62 is presently focusing on two-body final states, which should dominate for masses below 500 MeV. In this mode, the reconstruction of charged decay products allows both a determination of the invariant mass, and the measurement of the dark photon 3-momentum. The production point of the dark photon can then be inferred: for runs taken in a beam-dump configuration, it should be few interaction lengths within the most upstream TAX collimator; for runs taken in the standard configuration, a fraction of the dark photons may be produced in the Beryllium target, too. The expected sensitivity to dark photons di-lepton decays, evaluated from the sole contribution of the Beryllium target in the assumption of complete background rejection is shown in Fig 14, for a statistics of 10^{18} POT. At the moment, complete background rejection has been proven at 4×10^{15} POT for the di-muon final state, which is polluted by background due to accidental pairing of two muons from the beam halo. Including the contribution of dark photons produced in the TAX, NA62 should be able to explore free regions of the parameter space already with the statistics acquired in 2016

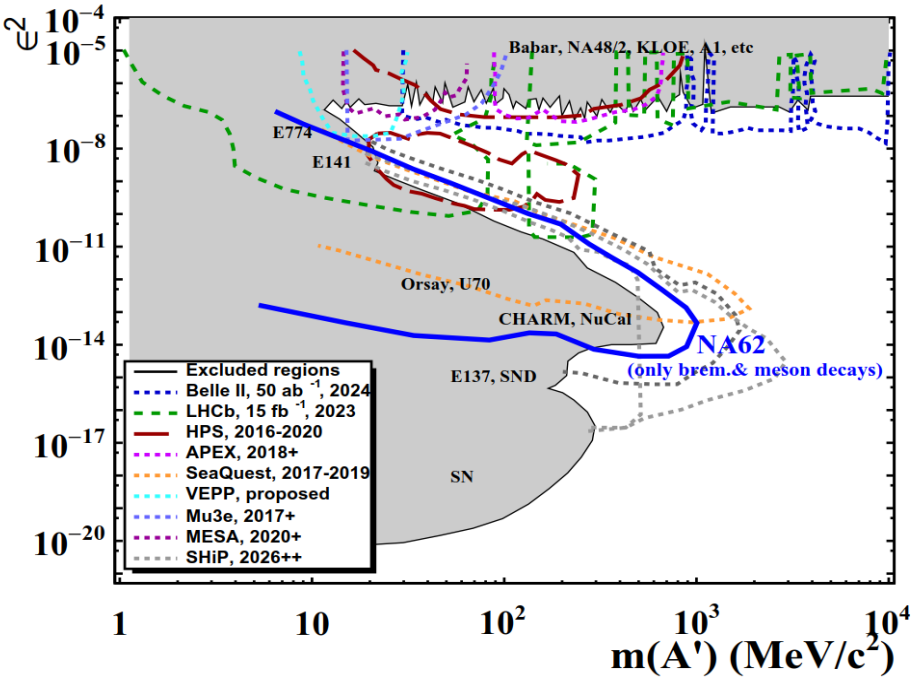

Figure 14: The NA62 expected sensitivity for dark photon di-leptonic decays, with a zero-background assumption, is shown by the blue line in terms of coupling to the SM photon (ϵ) vs dark photon mass ($m(A')$), for a statistics of 10^{18} protons on target.

6.2 Search for long-lived heavy neutral leptons

One of the reference models for heavy neutral leptons (HNL) in the MeV-GeV mass range is the neutrino minimal standard model [20]. In this model, three HNLs are added, with a certain freedom in terms of flavor couplings to the SM fields. To account for the observed baryon asymmetry in the universe, dark matter amount, and SM neutrino mixing, two of the HNL's are almost degenerate and with masses at the GeV level (the lightest HNL is a dark matter candidate with mass of the order of 10 keV). The heavy HNL's would be weakly coupled to the SM leptons and therefore be long lived. They would be emitted after proton-dump interactions by secondary mesons (kaons, charmed, and beauty mesons) and would subsequently decay in the fiducial volume. As for the dark photon, one might restrict the search to two-body decays, thus exploiting the total momentum reconstructed at the vertex, or to three-body open decays (with SM neutrinos in the final states). The sensitivity to the latter scenario is shown in Fig. 15, for a statistics of 10^{18} POT and assuming complete background rejection. Analysis of parasitically triggered data is in progress for the search of pion-muon final state.

6.3 Background study for final states with charged particles

The sensitivity to hidden sector particles originated from the dump can be greatly spoiled by the presence of background. In fact, the proton interactions on the dump, along with the signals, give rise to a copious direct production of short-lived resonances, and pions and kaons. While the length of the dump ($\sim 22\ \lambda_I$) is sufficient to absorb the hadrons and the electromagnetic radiation, the decays of pions, kaons and short-lived resonances result in a large flux of muons and neutrinos, which are the major sources of background in the apparatus.

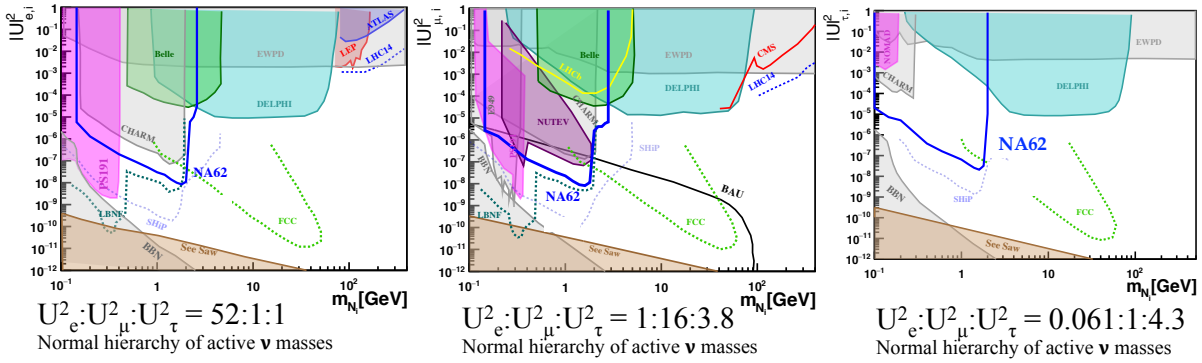

Figure 15: The NA62 expected sensitivity for heavy neutral leptons open decays, with a zero-background assumption, is shown by the blue line in terms of Yukawa coupling to the SM flavours vs mass, for a statistics of 10^{18} protons on target. The three scenarios shown are those in which the neutrino minimal standard model satisfies the bounds of the baryon asymmetry of the universe, of the observed dark matter amount and of the SM neutrino oscillations having the strongest Yukawa coupling for a certain flavour with respect to the other two [21]: electron (left panel), muon (central panel), and tau flavour (right panel).

About 18 kHz of muons have been measured at 40% nominal intensity in the NA62 acceptance in a ten-hour long run taken in dump mode, where about 2×10^{15} POT were recorded, and a preliminary study of the background rates and topologies has been performed. A simple selection has been applied to this sample to search for generic 2-track final states, requiring good quality tracks and 2-track vertices, no further activity in time with the two-track candidates, no additional track close to the selected vertices, and in-time coincidence of the two tracks at the CHOD. The reconstructed two-track vertex is required to lie in the interval $115 < z < 180$ m. Particle identification information has been used to study the background topologies.

The opposite-charge 2-track sample is the dangerous component as it can mimick a signal signature: it comprises random combinations of tracks from the muon halo and muon inelastic interactions in the last λ_I of the final collimator of the NA62 beam line, with one or no muons in the final state. In this category, the recontructed vertices are mostly concentrated at the beginning of the fiducial volume (Figure 16, left, red line) and the two tracks are mostly coincident in time. (Figure 16, center, red line).

Overall 28 events of the opposite-charge category are left after the selection. A powerful handle to further reduce the background while searching for fully reconstructed signal final states (eg: HNL decays to pion e/μ, Dark Photon or Dark scalar decay to oppositely charged particles e, μ, π, K) is to require the events to point backwards to the dump: as expected, all the events from the analyzed data sample do not satisfy this condition and can be removed by a mild cut in impact parameter. The extrapolation of the residual background tracks at the entrance of the decay vessel shows that they are all concentrated in a zone not covered by the current apparatus. The addition of an Upstream Veto upstream the fiducial volume with high efficiency and good time resolution would allow reduction of the background for 2-track final states open decays, which would be extremely relevant for the detection of HNL open modes [22].

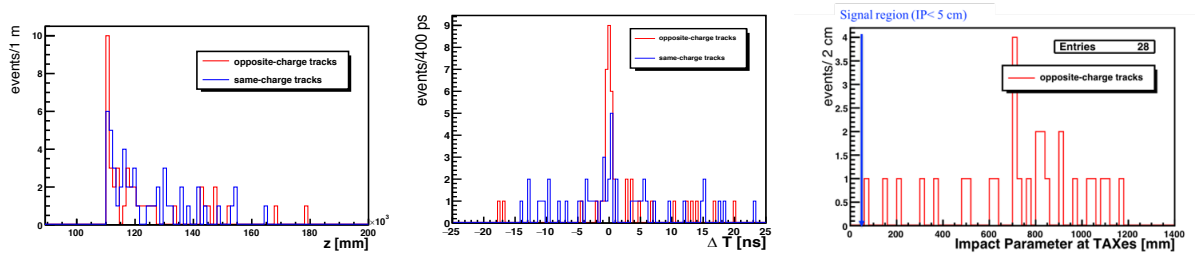

Figure 16: Left: $z-$distribution of the selected vertices for same-charge (blue line) and opposite-charge (red line) 2-track events. Center: arrival time difference at Charged Hodoscope (CHOD) of the selected two tracks for same-charge (blue line) and opposite-charge (red line) events. Right: impact parameter distribution of residual background events.

6.4 Search for long-lived axion-like particles

While dark photons and heavy neutral leptons can be searched for either in beam-dump or in standard data-taking, profiting in the former case of a lower background with respect to the latter, decays of ALPs to two photons can be isolated only using a beam-dump setup. The projected sensitivity to Primakoff-produced ALPs decaying to two photons [23] at NA62 is shown in Figure 17: in case of complete background rejection, a statistics of 10^{16} POT would be sufficient to explore new regions of the parameter space of coupling versus mass. The analysis of acquired data is in progress. The signal can be identified by exploiting the features of its expected, Primakoff-mediated production in terms of total photon energy vs polar angle of their energy-weighted barycenter.

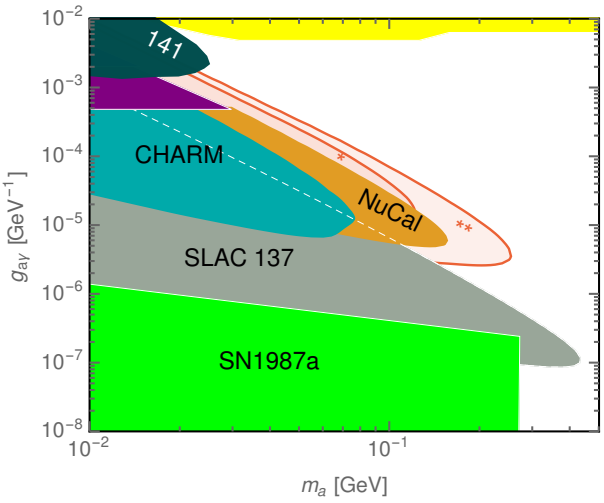

Figure 17: The NA62 expected sensitivity for ALP-to-two-photon search, with a zero-background assumption, in terms of ALP coupling vs ALP mass, for a number of protons on target equivalent to one day (red region marked with $*$, 1.3×10^{16} POT) and equivalent to one month (red region marked with $**$, 4×10^{17} POT) data takings.

Background rejection is paramount, so much effort has been devoted in isolating possible processes yielding two photon clusters in time with each other to within few ns: a simulation of the K12 line based on the G4BeamLine package [24] has been performed, to guide the search

for background sources. Possible mechanisms have been isolated, which are being cross checked with data, due to unswept muons from the beam halo reaching the NA62 fiducial volume. Halo muons can undergo bremstrahlung followed by pair production or can directly produce e^+e^- pairs in the passive material of the final collimator, few radiation lengths upstream its end part. Pair production events, as well as events with μ^+-electron or μ^--positron have been indeed isolated with data from the first row of Table 3. Electron-positron pairs can therefore start a shower, finally producing a pair of photons in time without additional charged activity in the event. Two mechanisms are at play: two photons can be radiated from the same particle, or one from each of the two. A simulation of the process based on data samples suggests that the few events populating an ALP signal sideband in the photon energy vs polar angle plane can be due to these two components.The determination of the absolute normalization for these background is in progress. The analysis is blind: after validation of the background in signal side bands, the signal box will be opened.

7 Publications of NA62 data and older data

Since the last NA62 SPSC review in April 2017, the collaboration has completed the publication of two physics analyses based on data sets recorded by NA62 in 2007 and 2015. The reference publication on the NA62 detector has been accepted and published by JINST.

- **Search for heavy neutral lepton production in K^+ decays**, E. Cortina Gil *et.al.*, NA62 Collaboration, published in Physics Letters B778 (2018) 137;
- **Search for heavy neutrinos in $K^+ \to \mu^+\nu_\mu$ decays**, C. Lazzeroni et al, NA62 Collaboration, published in Physics Letters B772 (2017) 712;
- **The beam and detector of the NA62 experiment at CERN**, The NA62 Collaboration, published in 2017 JINST 12 P05025 (May 2017).

More analyses based on the old 2003-2004 data of NA48/2 have been approved as preliminary results and are presented at Conferences while draft papers are being prepared for internal review and timely publication.

- Precision measurement of the K_{l3} Form Factors (NA48/2, 2004 Data);
- First observation and study of the $K^\pm \to \pi^\pm\pi^0 e^+e^-$ decay (NA48/2, 2003-2004 Data);
- Model independent measurement of the $K^\pm \to \mu^\pm\nu e^+e^-$ decay (NA48/2, 2003-2004 Data).

The collaboration is actively contributing to major International Conferences and topical Workshops with NA62 Detector contributions and recently published or preliminary physics results from NA62 and NA48/2 data analyses. In the past year (Mai 2017 to April 2018), the collaboration speakers presented 55 talks and 1 poster to Physics Conferences and 5 talks and 3 posters to Instrumentation Conferences. More contributions are already foreseen in future 2018 Conferences.

References

[1] The NA62 Collaboration, JINST **12** (2017) P05025

[2] R. Marchevski, 53rd Reconstres de Moriond - EW 2018, https://indico.in2p3.fr/event/16579/contributions/60808/attachments/47182/59257/Moriond_rmarchev.pdf.

[3] G. Ruggiero, CERN EP Seminar, 27/03/2018, https://indico.cern.ch/event/714178/attachments/1616653/2584699/seminar_ruggiero_cern018.pdf.

[4] A.J. Buras, D. Buttazzo, J. Girrbach-Noe and R. Knegjens, JHEP **1511** (2015) 33

[5] C. Patrignani *et al.* (Particle Data Group), Chin. Phys. **C40** (2016) 100001.

[6] A.L Read, J.Phys. **G28** (2002) 2693.

[7] W.A. Rolke, A.M. Lopez, Nucl. Instrum. Methods **A506** (2003) 250.

[8] A.V. Artamonov *et al.* (E949 collaboration), Phys. Rev. Lett. **101** (2008) 191802.

[9] A.V. Artamonov *et al.* (E949 collaboration), Phys. Rev. D **79** (2008) 092004.

[10] J.R. Batley *et al.* (NA48/2 collaboration), Phys. Lett. **B677** (2009) 246.

[11] R. Appel *al.* (BNL E865 collaboration), Phys. Rev. Lett. **83** (1999) 4482.

[12] R. Appel *al.* (BNL E865 collaboration), Phys. Rev. Lett. **85** (2000) 2877.

[13] J.R. Batley *et al.* (NA48/2 collaboration), Phys. Lett. **B697** (2011) 107.

[14] J.R. Batley *et al.* (NA48/2 collaboration), Phys. Lett. **B769** (2017) 67.

[15] A. Sher *et al.* (BNL E865 collaboration), Phys. Rev. **D72** (2005) 012005.

[16] V. Cirigliano and I. Rosell, Phys. Rev. Lett. **99** (2007) 231801.

[17] C. Lazzeroni *et al.* (NA62-2007 collaboration), Phys. Lett. **B719** (2013) 326.

[18] E. Cortina Gil *et al.* (NA62 collaboration), Phys. Lett. **B778** (2018) 137.

[19] L. B. Okun, Sov. Phys. JETP **56**, 502 (1982) [Zh. Eksp. Teor. Fiz. **83**, 892 (1982)]. For a comprehensive review, see J. Alexander *et al.*, arXiv:1608.08632 [hep-ph].

[20] T. Asaka, S. Blanchet and M. Shaposhnikov, Phys. Lett. B **631** (2005) 151.

[21] D. Gorbunov and M. Shaposhnikov, JHEP **0710** (2007) 015 Erratum: [JHEP **1311** (2013) 101].

[22] G. Lanfranchi [NA62 Collaboration], PoS EPS **-HEP2017**, 301 (2017).

[23] B. Döbrich, J. Jaeckel, F. Kahlhoefer, A. Ringwald and K. Schmidt-Hoberg, JHEP **1602**, 018 (2016).

[24] T.J.Roberts, et al., EPAC-2008-WEPP120, http://public.muonsinc.com/Projects/G4beamline.aspx